PHOTONICS Research

Robust hybrid laser linewidth reduction using Si_3N_4-based subwavelength hole defect assisted microring reflector

Jiachen Li,[1,2] Baoyu Zhang,[1,2] Sigang Yang,[1,2] Hongwei Chen,[1,2] and Minghua Chen[1,2,*]

[1]Beijing National Research Center for Information Science and Technology (BNRist), Beijing 100084, China
[2]Department of Electronic Engineering, Tsinghua University, Beijing 100084, China
*Corresponding author: chenmh@tsinghua.edu.cn

Received 12 October 2020; revised 6 February 2021; accepted 7 February 2021; posted 8 February 2021 (Doc. ID 412284); published 26 March 2021

We demonstrate a hybrid laser with a low intrinsic linewidth of 34.2 Hz and a high fiber-coupled output power of 11.7 dBm, by coupling a Si_3N_4-based subwavelength hole defect assisted microring reflector (SHDA-MRR) to a commercially available distributed feedback semiconductor laser. The proposed SHDA-MRR structure features an accurately controlled reflection response, with the manipulated modal coupling between two degenerate counterpropagating modes induced by a subwavelength hole defect embedded in the microring waveguide. With further joint optimization of cavity parameters, this Si_3N_4 SHDA-MRR structure is expected to reduce the laser intrinsic linewidth to a sub-hertz level. This work explores a low-cost and robust linewidth reduction scheme for the applications of high-speed coherent optical communications systems and high-resolution optical metrology.

https://doi.org/10.1364/PRJ.412284

1. INTRODUCTION

Narrow-linewidth lasers are key elements for a wide range of applications that require extreme coherence length or high spectral purity, such as high-speed coherent optical communications systems [1], high-resolution spectroscopy [2], high-resolution optical sensing [3], ultraprecise timing [4], and spectrally pure photonic microwave generation [5]. Although current commercial solid-state lasers [6] or fiber lasers [7] have exhibited high performance, these devices are generally composed of discrete components with large footprints that are a challenge to integrate with other on-chip optical microsystems. Therefore, for those applications where size, weight, and power (SWaP) are critical operational parameters, the chip-scale semiconductor laser is a more favorable choice. However, limited to the low-quality-factor laser cavity due to the small size, traditional monolithic III-V semiconductor lasers have demonstrated the best linewidth in the tens of kilohertz and mostly in the megahertz level [8], which can not fully meet the requirements of narrow linewidth for the aforementioned applications.

In recent years, there has been significant interest in reducing the laser linewidth by using the on-chip low-loss passive resonator to increase the photon lifetime of the laser cavity [9]. These chip-scale narrow-linewidth lasers have been developed by heterogeneously integrating III-V gain materials along with the low-loss passive waveguide on the same chip [10,11] or butt-coupling the III-V gain chip to the external cavity on a silicon [12,13] or silicon nitride (Si_3N_4) [14–19] waveguide platform. From a performance standpoint, in contrast with silicon, a Si_3N_4 platform has several advantages. The low waveguide propagating loss [20] leads to an extremely extended photon lifetime, resulting in a better linewidth reduction performance. Besides, Si_3N_4 is not limited by the two-photon absorption effect [21], thus supporting higher on-chip light power. Compared with silicon, Si_3N_4 features wider transparency [22], enabling applications in different optical bands.

In this paper, we report a Si_3N_4-based subwavelength hole defect assisted microring reflector (SHDA-MRR) structure as an on-chip feedback cavity for hybrid self-injection-based [23] laser linewidth reduction. With the embedded subwavelength hole defect in the SHDA-MRR waveguide, part of the incident light is scattered backward into its counterpropagating mode, leading to an enhanced coherent buildup of the reflected light and a manipulated inter-cavity modal coupling. Based on our theoretical model, the reflection response of the SHDA-MRR can be accurately controlled by designing the hole-defect size. Different from ultra-high-Q whispering gallery mode microresonators (WGMRs) [18,24,25], where the reflected light is excited by the intrinsic inter-cavity backscattering induced by the sidewall roughness [26], the proposed SHDA-MRR features a flexible and manipulated reflection response. In particular, we have fabricated the proposed SHDA-MRR on the

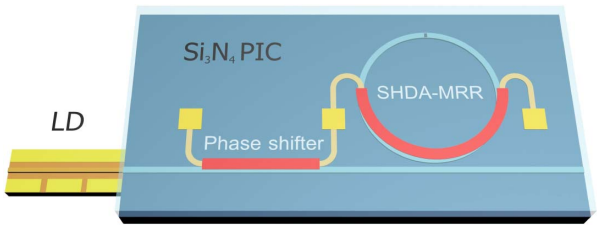

Fig. 1. Schematic diagram of the proposed hybrid narrow-linewidth laser with a Si_3N_4-based SHDA-MRR as an external feedback cavity butt-coupled with a commercially available DFB laser diode (LD).

low-loss Si_3N_4 waveguide platform and experimentally verified its reflection response. Using this Si_3N_4-based SHDA-MRR as an external reflector butt-coupled with a commercially available distributed feedback (DFB) semiconductor laser, we have demonstrated a hybrid self-injection-based narrow-linewidth laser (see Fig. 1), with its intrinsic linewidth significantly suppressed from 49.6 kHz to 34.2 Hz. Besides, the demonstrated laser exhibits a large side mode suppression ratio (SMSR) of 50 dB and high fiber-coupled output power of 11.7 dBm without a booster semiconductor optical amplifier (SOA). With further joint optimization of cavity parameters, this Si_3N_4 SHDA-MRR is expected to reduce the laser intrinsic linewidth to a sub-hertz level.

2. PRINCIPLE OF SHDA-MRR

The schematic configuration of the proposed SHDA-MRR structure is illustrated in Fig. 2. Typically, there is no reflected light at the input port for an ideal traveling-wave all-pass microring resonator. However, in SHDA-MRR, we introduce a subwavelength hole defect in the microring waveguide of a conventional all-pass microring resonator as a manipulated backward scattering point to break its unidirectionality. When the incident light coupled from the input port propagates through this subwavelength hole defect, a fraction of the

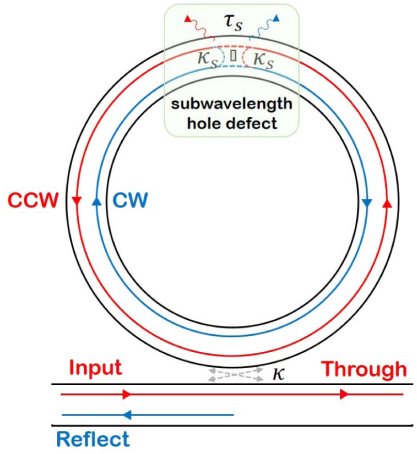

Fig. 2. Schematic diagram of the proposed SHDA-MRR structure (not to scale). A subwavelength hole defect is embedded in the microring waveguide of a conventional all-pass microring resonator for generating manipulated backward scattering and inter-cavity modal coupling between CW and CCW modes.

counterclockwise (CCW) mode is scattered backward to excite its degenerate clockwise (CW) mode, indicated as the backward scattering coefficient. Because of the periodic nature of the ring structure, this minor backscattering can lead to an enhanced coherent buildup of the CW mode, even if the individual reflection is weak. With the same backward scattering coefficient, the CW mode can also be reflected back into the CCW mode. Therefore, the degenerate CCW and CW modes become mutually coupled into two new resonance states with a mixed CW/CCW nature [26], because they are inherently phase-matched by the same subwavelength-hole-defect-induced backscattering. Such a manipulated inter-cavity modal coupling ultimately leads to two beneficial effects: it breaks the unidirectionality of an all-pass microring resonator and causes the desired reflected light at the input port, and it provides the possibility of controlling the reflection response by designing the subwavelength-hole-defect-induced backward scattering coefficient. Hence, this proposed SHDA-MRR structure is appropriate to be employed as an on-chip wavelength-selective reflector for the compact hybrid self-injection-based laser linewidth reduction.

To support the above analysis, we built a transfer-matrix-based [27] theoretical model for calculating spectral transmission responses of the SHDA-MRR. Assuming there is no radiation loss in the microring coupling region, and the intrinsic backscattering [26] induced by the sidewall roughness and the waveguide coupling is negligible relative to subwavelength-hole-defect-induced backscattering, the optical-field transmission functions of reflection and through responses are obtained and shown in the following equations:

$$H_{\text{reflection}} = -\frac{i\kappa_s\kappa^2}{\tau_s a^2(1-\kappa^2) - 2a\sqrt{1-\kappa^2}\sqrt{\tau_s-\kappa_s^2}+1}, \quad \textbf{(1)}$$

$$H_{\text{through}} = -\frac{\tau_s a^2\sqrt{1-\kappa^2} - a(2-\kappa^2)\sqrt{\tau_s-\kappa_s^2}+\sqrt{1-\kappa^2}}{\tau_s a^2(1-\kappa^2) - 2a\sqrt{1-\kappa^2}\sqrt{\tau_s-\kappa_s^2}+1}. \quad \textbf{(2)}$$

In the above equations, κ_s and τ_s are the subwavelength-hole-defect-induced backward scattering coefficient and scattering loss coefficient, κ is the optical-field coupling coefficient in the microring-waveguide coupling region, and $a = e^{-\alpha L_c}e^{i\frac{2\pi n L_c}{\lambda}}$ is the round-trip complex transmission coefficient. Here, α is the optical-field propagating loss coefficient, L_c is the perimeter of the microring resonator, n is the effective refractive index, and λ is the incident light wavelength. It should be noted that the location of the inserted subwavelength hole defect has no impact on transmission responses of the SHDA-MRR, which can be confirmed in Eqs. (1) and (2).

Based on the proposed theoretical model, we plot the simulated transmission spectra of the SHDA-MRR in Fig. 3(a), with parameters of $\kappa_s = 0.0064$, $\kappa = 0.2$, $\tau_s = 0.999$, $|a| = 0.998$, and $nL_c = 5600$ μm. With this manipulated backward scattering, the SHDA-MRR presents an effective reflection response, which is not supported in a standard all-pass microring resonator [Fig. 3(c)]. Due to the inter-cavity modal coupling between CW and CCW modes, this reflection response differs from the Lorentzian line shape [28] of the commonly used inline reflector based on an add-drop microring resonator

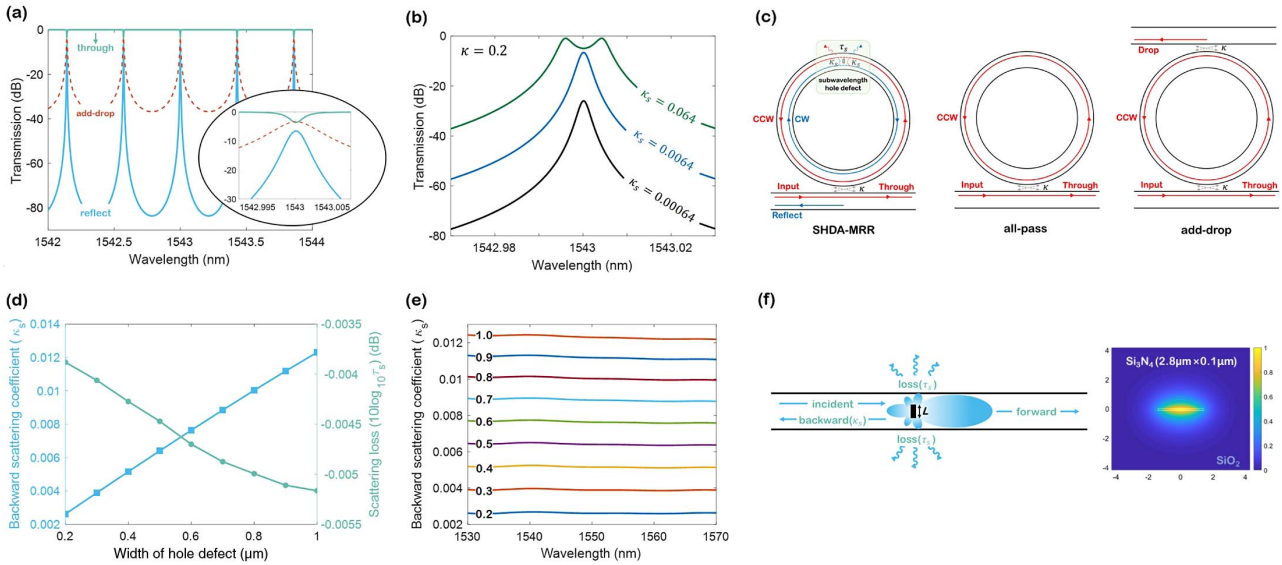

Fig. 3. (a) Simulated transmission spectra (including reflection and through responses) of the SHDA-MRR and corresponding reflection response of an add-drop microring reflector (dashed line) for comparison. (b) Simulated reflection responses of the SHDA-MRR with different κ_s (with κ fixed at 0.2). (c) Comparison of the SHDA-MRR configuration, with the all-pass microring configuration and the add-drop microring configuration. (d) Simulation of κ_s and τ_s (at 1543 nm) induced by the subwavelength hole defect with various sizes (the hole-defect length is fixed at 0.2 μm and the hole-defect width is varied from 0.2 to 1.0 μm). (e) κ_s with the simulation wavelength varying from 1530 to 1570 nm. (f) Schematic diagram of the etched subwavelength hole defect in the waveguide for the simulation in (d) and (e). The simulation is based on the fundamental-TE-mode Si_3N_4 waveguide (100 nm thick and 2.8 μm wide) with SiO_2 cladding, and its mode profile is shown on the right.

[Fig. 3(c)] [19,29], which is also simulated with the same parameters for comparison [dashed line in Fig. 3(a)]. From the zoomed spectra around a resonance wavelength, the reflection response of the SHDA-MRR shows a significantly enhanced edge steepness and a larger sidelobe extinction ratio, in contrast with the conventional Lorentzian line shape. Moreover, the reflection bandwidth of the SHDA-MRR is much narrower than that of an add-drop microring reflector with the same coupling coefficient. That is because the SHDA-MRR has only a single coupler to couple light between the microring resonator and the bus waveguide, in contrast to a more commonly used add-drop microring reflector formed by two couplers [see Fig. 3(c)]. Therefore, the SHDA-MRR has shown its unique superiority as a wavelength-selective feedback cavity for the laser linewidth reduction, compared with the standard add-drop microring reflector. On the one hand, its steeper edge and excellent sidelobe extinction ratio result in a better SMSR of the hybrid laser. On the other hand, the narrowband reflection resonance of the SHDA-MRR leads to a considerable linewidth suppression [23].

Notably, for SHDA-MRR, different reflection responses can be obtained by designing the backward scattering coefficient (κ_s), as shown in Fig. 3(b). When $\kappa_s = 0.00064$, this relatively small backscattering induced by the subwavelength hole defect results in the insufficient buildup of the CW mode and the weak inter-cavity modal coupling between CW and CCW modes. In this case, the SHDA-MRR is not suitable as an external reflector for the self-injection-based hybrid laser because of the low reflection strength. With κ_s increasing from 0.00064 to 0.064, the reflection strength of the SHDA-MRR is gradually enhanced but reaches an eventual saturation as the modal coupling between CW and CCW modes becomes strong. For instance, when $\kappa_s = 0.064$, the resonant peak of the reflection response obviously splits, due to the entirely broken degeneracy of two counterpropagating modes [30]. However, based on relevant studies [31], this larger resonance splitting impacts the self-injection locking process and worsens the frequency stabilization performance. Therefore, in SHDA-MRR, we should choose a reasonable backward scattering coefficient (κ_s) to achieve the desired reflection response for the good-performance self-injection locking process and linewidth reduction.

For an accurate and flexible backward scattering coefficient, we propose that the inter-cavity backscattering and the modal coupling can be manipulated by etching a subwavelength hole defect with varied sizes in the microring waveguide. To verify this statement, we simulate κ_s and τ_s with various hole-defect sizes in the fundamental-TE-mode Si_3N_4 waveguide (2.8 μm wide and 0.1 μm thick) with SiO_2 cladding [see Fig. 3(f)], by employing the three-dimensional finite-difference time-domain (3D-FDTD) method. In this simulation, we fix the hole-defect length at 0.2 μm and change the hole-defect width. As shown in Fig. 3(d), with the hole-defect width (L) increasing from 0.2 to 1.0 μm, the backward scattering coefficient κ_s gradually increases from 0.0026 to 0.0123. However, the scattering loss simultaneously becomes larger with the enhancement of the subwavelength-hole-defect-induced backscattering. As shown in Fig. 3(e), the subwavelength-hole-defect-induced backscattering is basically maintained within the wavelength ranging from 1530 to 1570 nm. In summary, based on the above simulation results, this subwavelength hole defect etched in the microring waveguide provides a feasible scheme for generating the manipulated inter-cavity backscattering. Compared to the

commonly used high-Q WGMRs [18,24,25], where the intrinsic inter-cavity Rayleigh scattering induces the modal coupling between CW and CCW modes, the SHDA-MRR features a flexible and adjustable subwavelength-hole-defect-induced backward scattering coefficient.

3. EXPERIMENT AND RESULTS

A. Si_3N_4-Based SHDA-MRR Chip

We have fabricated the proposed SHDA-MRR structure on the Si_3N_4 waveguide platform and demonstrated its performance as an external feedback cavity for the hybrid narrow-linewidth laser. The fabrication process starts from a Si wafer with a 10 μm thick SiO_2 (thermal oxide) layer. A 0.1 μm thick Si_3N_4 layer is grown by low-press chemical vapor deposition (LPCVD). The Si_3N_4 waveguide is patterned and etched using deep-UV (DUV) stepper lithography and reactive ion etching (RIE), respectively. Then, a first 2 μm thick SiO_2 cladding is formed by LPCVD, and a second 6 μm thick SiO_2 cladding is formed by plasma-enhanced chemical vapor deposition (PECVD). In the fabrication process, the device is fully annealed to remove hydrogen impurities [18] and reduce the waveguide absorption loss. To thermally tune the SHDA-MRR reflection resonance, TiN heaters are deposited and patterned over the top SiO_2 layer. The detailed cross section of this employed Si_3N_4 waveguide platform is shown in Fig. 4 (bottom, right), and its mode profile of the fundamental mode is simulated in Fig. 3(f).

As displayed in the optical microscope image in Fig. 4, the width of the single-mode Si_3N_4 waveguide for the wavelength of 1550 nm is set to be 2.8 μm, and the radius of the SHDA-MRR is set to be 600 μm. Based on the simulation results in Figs. 3(a) and 3(d), a strip-type hole defect with the size 0.5 μm × 0.2 μm is etched in this SHDA-MRR waveguide for $\kappa_s = 0.0064$, and the microring coupling gap is designed to be 0.9 μm for $\kappa = 0.2$. This introduced subwavelength hole defect is specifically designed to be located far away from the coupling section to avoid influencing the light coupling between the microring and the bus waveguide. Moreover, a phase shifter of 800 μm is placed adjacent to the SHDA-MRR to achieve the phase-matching condition [31], for facilitating the best self-injection locking process.

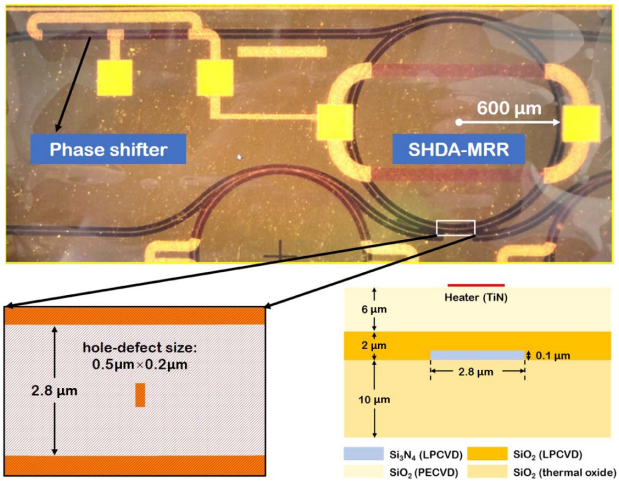

Fig. 4. Optical microscope image of the fabricated Si_3N_4-based SHDA-MRR chip for the laser linewidth reduction. A subwavelength hole defect with the size 0.5 μm × 0.2 μm is etched in the waveguide (bottom, left). Cross section (not to scale) of the employed Si_3N_4 waveguide platform is also shown (bottom, right).

Here, we have three main reasons for choosing this Si_3N_4 waveguide platform to demonstrate the SHDA-MRR: the low propagation loss of this high-aspect-ratio Si_3N_4 waveguide [32–34] leads to a higher loaded Q (Q_L) of the SHDA-MRR, which generally means a narrower intrinsic linewidth of a self-injection-based hybrid laser; the broad transparency (~400–2350 nm) [22] of Si_3N_4 makes the SHDA-MRR structure applicable for the laser linewidth reduction over an extremely wide wavelength range; and the relatively low thermal drift coefficient of the Si_3N_4 waveguide [35] helps to improve the long-term stability of the hybrid laser under self-injection locking [25].

We experimentally characterize the fabricated Si_3N_4-based SHDA-MRR by measuring its transmission spectra. Here, we use the high-numerical-aperture UHNA3 fiber with a small mode-field-diameter (MFD) of 4.1 μm for the high-efficiency fiber-to-waveguide coupling of 2 dB/facet [36] and employ an advanced optical spectrum analyzer (OSA, APEX, AP2081B, resolution of 20 MHz) with a built-in tunable laser to measure its reflection and through responses. Figure 5(a) shows measured transmission spectra around a resonance wavelength. The 3 dB bandwidth of the reflection resonance is 244 MHz, corresponding to a Q_L of 8×10^5, and the insertion loss of this reflection response is measured to be −7 dB. On resonance, the reflection line shape exhibits an enhanced extinction ratio with a large slope rate of 5900 dB/nm (6 dB offset from the resonant peak). By fitting these measured spectra to the theoretical model [based on Eqs. (1) and (2), shown with dashed lines],

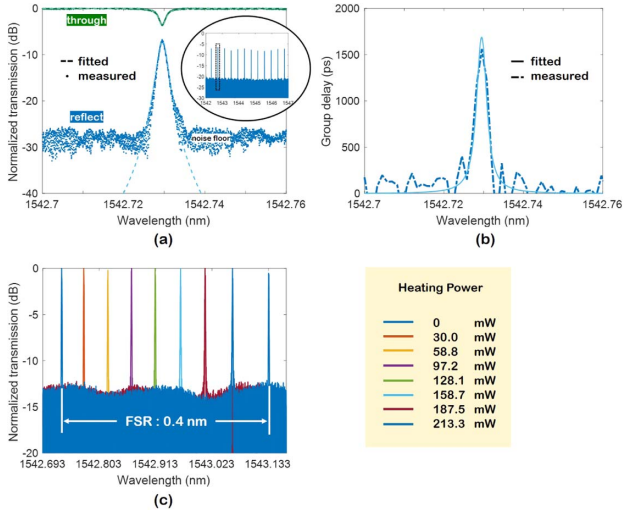

Fig. 5. (a) Measured (dots) and fitted [dashed lines, by Eqs. (1) and (2)] transmission spectra (reflection and through responses) of the fabricated Si_3N_4-based SHDA-MRR. The inset shows flat multiple reflection resonances from 1542 to 1547 nm, with an FSR of 0.4 nm. (b) Measured (dashed line) and fitted [solid, by Eq. (1)] group delay of the fabricated Si_3N_4-based SHDA-MRR. (c) Measured reflection resonance tuning across one FSR, with an increased heating power applied to the microheater.

the key parameters in the model are extracted as $\kappa_s = 0.0056$, $\tau_s = 0.999$, and $\kappa = 0.19$. The Si_3N_4 waveguide propagation loss is fitted to be 4.4 dB/m, corresponding to an intrinsic Q (Q_0) of 5.1×10^6. From the inset of Fig. 5(a), we observe nearly flat multiple reflection resonances from 1542 to 1547 nm, with a free spectral range (FSR) of 0.4 nm. We further employ an optical vector analyzer (LUNA, OVA 5000) with a resolution of 1.25 pm to measure the group delay of the fabricated device. As shown in Fig. 5(b), the group delay at the reflection response of the SHDA-MRR is measured and fitted to be 1.68 ns, equivalent to an effective delay length of 0.32 m. All of the above experimental results accord well with the design values and the simulation results shown in Fig. 3. Moreover, we measure the reflection resonance tuning with an increased heating power applied to the microheater over the SHDA-MRR. As shown in Fig. 5(c), the reflection resonance is tuned across one FSR, and the resonance line shape can be well maintained. Therefore, with the periodic reflection responses (FSR = 0.4 nm) and the thermal tuning, we can align a reflection resonance of the SHDA-MRR to any desired wavelength for the robust self-injection-based laser linewidth reduction.

B. Hybrid Narrow-Linewidth Laser with SHDA-MRR

We demonstrate a hybrid narrow-linewidth laser [see Fig. 6(a)] by edge coupling the fabricated Si_3N_4-based SHDA-MRR chip to a commercially available high-power DFB semiconductor

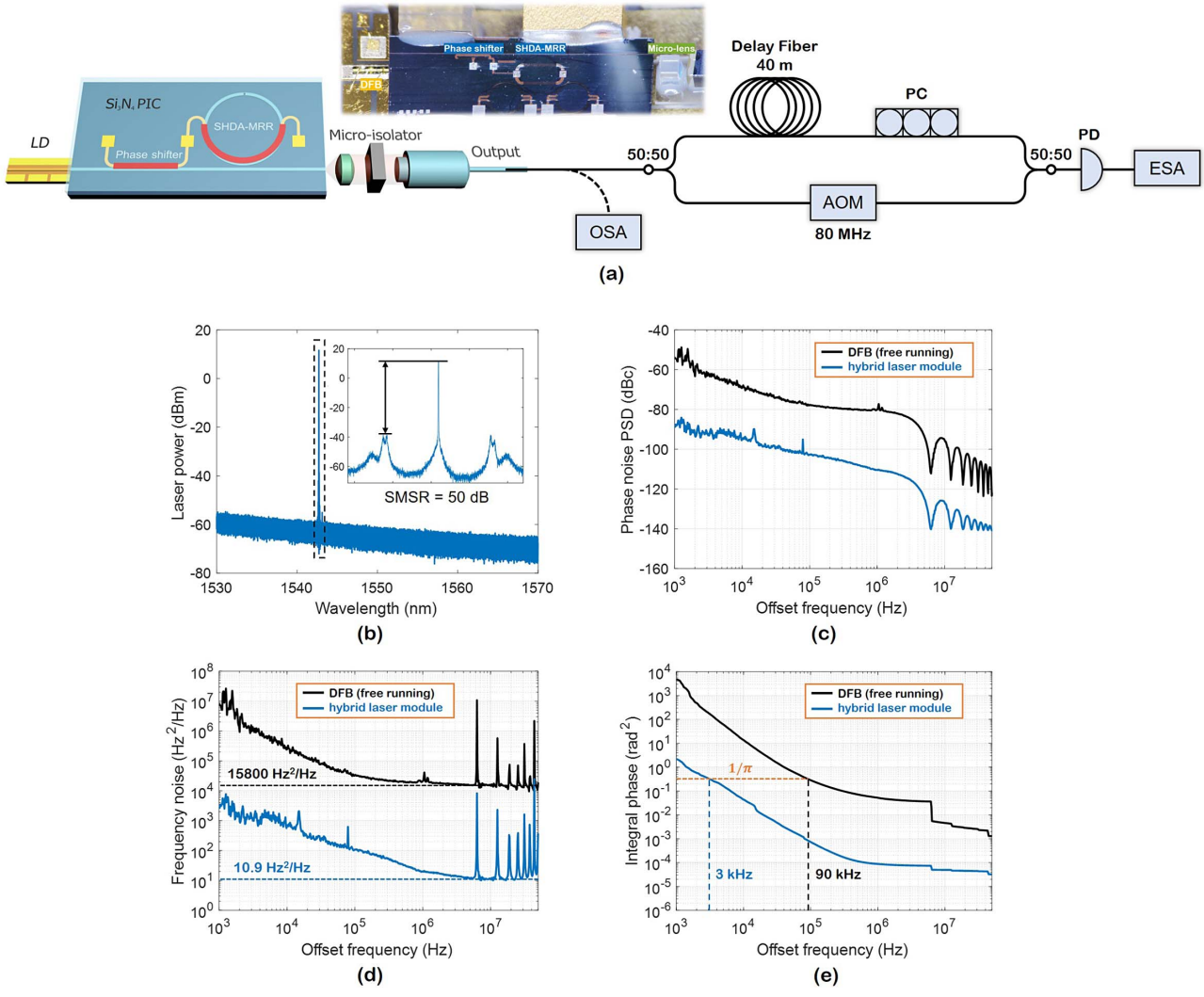

Fig. 6. (a) Schematic diagram of the experimental setup. A Si_3N_4-based SHDA-MRR is butt-coupled with a commercially available DFB semiconductor laser for a hybrid narrow-linewidth laser. The output light from the chip is collected and collimated by the micro-lens, and a micro-isolator is placed behind the micro-lens. The inset shows the zoom-in photo of the packaged laser module. The laser output is sent into a DSH setup for the phase noise PSD measurement. LD, laser diode; PD, photodiode; PC, polarization controller; AOM, acousto-optic modulator; OSA, optical spectrum analyzer; ESA, electrical signal analyzer (Agilent E5052). (b) Measured optical spectrum of the hybrid narrow-linewidth laser. The inset shows an SMSR of 50 dB. (c) Single-sided phase noise PSD of the free-running DFB laser and the hybrid laser based on the Si_3N_4 SHDA-MRR. (d) Frequency noise spectra of the free-running DFB laser (showing a white noise floor of 15,800 Hz^2/Hz corresponding to 49.6 kHz intrinsic linewidth) and the hybrid laser based on the Si_3N_4 SHDA-MRR (showing a white noise floor of 10.9 Hz^2/Hz corresponding to 34.2 Hz intrinsic linewidth). (e) Integral phase noise spectra of the free-running DFB laser and the hybrid laser based on the Si_3N_4 SHDA-MRR calculated from the measured frequency noise spectra. Integral linewidths of 90 kHz and 3 kHz are extracted, respectively.

laser chip. The DFB laser provides a single-mode output light of 17 dBm near 1543 nm with a typical injection current of 200 mA. In the experiment, the coupling loss between the DFB laser and the Si_3N_4-based SHDA-MRR chip is measured to be −2.5 dB, and this coupling loss can be further improved to less than −1 dB by optimizing the misalignment and separation between the two chips [13,37]. The output light from the Si_3N_4 chip is collimated and collected by a micro-lens and a fiber collimator. A micro-isolator is placed behind the micro-lens for immuning the external reflection. The hybrid laser module is packaged on a temperature-controlled [by 5305 TECSource (0.004°C stability over one hour), Arroyo Instruments] submount, as shown in the inset of Fig. 6(a).

We employ the OSA to measure the lasing spectrum of the hybrid laser, with the DFB laser (injection current of 200 mA) self-injection locked to a reflection resonance of the SHDA-MRR. As shown in Fig. 6(b), the demonstrated hybrid laser exhibits an enhanced SMSR of 50 dB, compared with the 45 dB SMSR of the free-running DFB laser. Due to the SHDA-MRR induced on-chip loss (under the self-injection locking) of 1 dB and the chip-fiber coupling loss of 1.8 dB, the actual fiber-coupled output power is measured to be 11.7 dBm, and the on-chip power is estimated to be 13.5 dBm.

To characterize the performance of this fabricated Si_3N_4 SHDA-MRR on the self-injection-based laser linewidth reduction, we measure the phase noise power spectral density (PSD) [38] of the hybrid laser and the free-running DFB laser, using the delayed self-heterodyne (DSH) method [8], as shown schematically in Fig. 6(a). In the DSH configuration, the laser output is sent to a fiber interferometer with a delay fiber of 40 m in one path, which is much shorter than the laser coherence length. In another path, an acousto-optic modulator is used to generate a frequency shift of 80 MHz. The radio-frequency (RF) beat signal from the photodiode is evaluated with an electrical signal analyzer (Agilent E5052). With this scheme, the fluctuations of the instantaneous laser frequency are converted to fluctuations of interferometer output amplitude [8]. Compared with another widely used DSH technique with a large fiber delay longer than the laser coherence time, our employed method is less susceptible to technical noises from the surrounding environment. We obtain the laser single-sided phase noise PSD [$L_{\Delta\phi}(f)$] from the directly measured phase noise PSD [$S_{\Delta\phi}(f) = 2L_{\Delta\phi}(f)$] of RF beat signals, as shown in Fig. 6(c). Compared to the free-running DFB laser, the corresponding hybrid laser's single-sided phase noise is significantly suppressed to −88.7 dBc from −54 dBc, at the frequency offset of 1 kHz. The laser frequency noise PSD [$S_\nu(f)$] is related to the directly measured $S_{\Delta\phi}(f)$ by the following equation [38]:

$$S_\nu(f) = \frac{f^2}{4[\sin(\pi f \tau)]^2} S_{\Delta\phi}(f), \tag{3}$$

and the delay τ in the DSH setup is extracted as 159 ns from the measured phase noise spectra. Based on the laser frequency noise PSD, the laser intrinsic linewidth (quantum-limited Lorentzian linewidth) can be accurately acquired as $\Delta\nu_{\text{Lorentzian}} = \pi S_\nu^0$; here S_ν^0 is the white frequency floor at higher frequencies [8], where the measurement is free from the $1/f$ noise [39] and other typical technical noises [8,25]. The frequency noise spectra shown in Fig. 6(d) indicate white noise floors of 15,800 Hz^2/Hz for the free-running DFB laser, and 10.9 Hz^2/Hz for the hybrid laser, corresponding to 49.6 kHz and 34.2 Hz intrinsic linewidths, respectively. Therefore, the fabricated Si_3N_4-based SHDA-MRR has been demonstrated to suppress the DFB laser intrinsic linewidth by about 1450 with the self-injection locking, corresponding to a linewidth reduction factor η calculated to be $\sqrt{1450} \approx 38.1$.

The theoretical model of a single-mode semiconductor laser coupled to an external wavelength-selective feedback cavity has been well studied [40–42], and the maximum efficiency of self-injection locking can be approximated by the following expression [40]:

$$\eta = 1 + \sqrt{(1 + \alpha_H^2)\frac{P_r}{P_0}}\frac{\tau_{\text{SHDA-MRR}}}{\tau_{\text{cold}}}. \tag{4}$$

The laser intrinsic linewidth can be reduced by η^2. Here, α_H is the linewidth enhancement factor [43], $\tau_{\text{SHDA-MRR}}$ and τ_{cold} are the effective delay time provided by the Si_3N_4 SHDA-MRR chip and the DFB laser cavity, and P_r/P_0 represents the power ratio reflected back to the DFB laser (including the coupling loss). Based on the above experimental demonstration, the variables in Eq. (4) are reasonably estimated to be $\alpha_H = 2.5$, $P_r/P_0 = -12$ dB, $\tau_{\text{SHDA-MRR}} = 1.7$ ns, and $\tau_{\text{cold}} = 16$ ps, and the theoretical linewidth reduction factor η is calculated to be 72.8. The experimentally demonstrated η is a bit lower than the theoretical value obtained by Eq. (4), and one possible reason is that we have not tuned the self-injection locking process to the optimal locking phase or the optimal locking point, which has been discussed in detail in Ref. [31].

Such a high-power hybrid laser with an ultranarrow intrinsic linewidth is required as a critical component in high-speed coherent optical communications systems [1], where the laser frequency noise at high frequencies is of more importance, for low-phase-error coherent communication links. However, for many metrology applications, such as high-resolution spectroscopy [2], high-resolution optical sensing [3], and light detection and ranging (lidar) [44], the frequency noise at low frequencies eventually limits the metrology resolution. Therefore, in these applications, the full width at half-maximum (FWHM) linewidth (also known as the integral linewidth) can be of major importance. The integral linewidth [8] represents the "slow linewidth" obtained after a long-time averaging, and this measurement comprises technical noises in the low-frequency range, such as noises from the thermal drift and fluctuations of the injection current.

The laser integral linewidth ($\Delta\nu_{\text{int}}$) can be determined from the laser frequency noise PSD by the following expression [8]:

$$\int_{\Delta\nu_{\text{int}}}^{\infty} \frac{S_\nu(f)}{f^2} \mathrm{d}f = \frac{1}{\pi}(\text{rad}^2). \tag{5}$$

As shown in the calculated integral phase noise spectra in Fig. 6(e), integral linewidths of the free-running DFB laser and the hybrid laser are estimated to be 90 and 3 kHz, respectively. Thus, the fabricated Si_3N_4-based SHDA-MRR is demonstrated to suppress the DFB laser integral linewidth by about

30 with the self-injection locking. However, limited by the $1/f$ noise and other technical noises in the low-frequency range [8,39], the performance of the SHDA-MRR for realizing the integral linewidth reduction is not as good as the aforementioned experimental results about intrinsic linewidth reduction. This can be further improved by optically locking the hybrid laser to another high-Q etalon using Pound–Drever–Hall (PDH) techniques to suppress the laser frequency noise in the low-frequency range [45].

4. DISCUSSION

In conventional self-injection schemes based on high-Q WGMRs [33,46], the intrinsic inter-cavity backscattering induced by the sidewall roughness is used to generate the reflected light and thus makes the intrinsic backscattering strength hard to manipulate [31]. In contrast with the commonly used schemes, the proposed SHDA-MRR structure features a flexible and controllable backward scattering coefficient, by designing the size of the subwavelength hole defect etched in the microring waveguide. Therefore, we can further optimize the reflection response of the SHDA-MRR for the self-injection locking to achieve a better linewidth reduction performance, by optimizing κ and κ_s jointly. In Fig. 7, we calculate the linewidth reduction factor η [based on Eq. (4)] by simulating different SHDA-MRR reflection responses [by Eq. (1)] with various κ and κ_s (other parameters are the same as the experimentally demonstrated Si_3N_4 SHDA-MRR chip). According to our analysis, a sub-hertz intrinsic linewidth should be achievable with optimal κ and κ_s. For instance, for the experimentally demonstrated κ_s of 0.0056 in the fabricated Si_3N_4 SHDA-MRR, a lower $\kappa \in [0.05, 0.1]$ is preferred for a better linewidth reduction performance. Moreover, from Fig. 7, the increase of κ_s above some optimal value (with κ unchanged) does not always provide a better linewidth reduction. Based on Fig. 3(b), a larger κ_s can result in the obvious resonance splitting and then

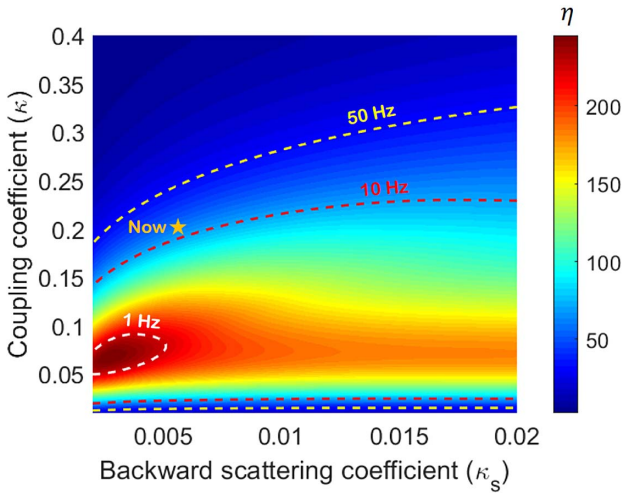

Fig. 7. Calculated linewidth reduction factor η [based on Eq. (4)] by simulating different SHDA-MRR reflection responses [based on Eq. (1)] with various κ and κ_s. With the optimized κ and κ_s, the hybrid laser based on the Si_3N_4 SHDA-MRR has the potential to reach a sub-hertz intrinsic linewidth.

worsen the self-injection stabilization performance [31]. Besides, it is an effective path to obtain a better self-injection-based linewidth reduction and output power by further optimizing the chip-to-chip coupling loss. In addition to the proposed SHDA-MRR structure, some other structures [47–49] can also be employed to tailor the cavity backscattering and reflection line shape with the manipulation of backreflection and backcoupling in the cavity.

As shown in Fig. 5, the SHDA-MRR features periodic resonances with an FSR of 0.4 nm, and each reflection resonance can be continuously tuned across one FSR using the thermo-optic effect. Therefore, we can lock a reflection resonance of the SHDA-MRR to the DFB laser at arbitrary wavelengths. Moreover, due to the broad transparency of the Si_3N_4, the SHDA-MRR can be designed to be applied in different optical bands. Thus, the Si_3N_4-based SHDA-MRR has provided a robust solution to realize the hybrid linewidth reduction.

5. CONCLUSIONS

In conclusion, we have demonstrated a hybrid integrated laser with 34.2 Hz intrinsic and 3 kHz integral linewidths, based on the proposed Si_3N_4 SHDA-MRR structure for the self-injection locking. The hybrid laser exhibits a large SMSR of 50 dB and high fiber-coupled output power of 11.7 dBm. In SHDA-MRR, the reflection response can be accurately manipulated by designing the size of the embedded subwavelength hole defect. With further joint optimization of cavity parameters, this Si_3N_4 SHDA-MRR is expected to reduce the laser intrinsic linewidth to a sub-hertz level. Therefore, this work explores a low-cost and robust linewidth reduction scheme based on the commercially available DFB laser, for the applications of high-speed coherent optical communications systems, high-resolution optical sensing, and lidar. Substituting the DFB laser with a Fabry–Perot semiconductor laser [19], the hybrid laser has the potential to reach a widely tunable single-longitudinal-mode output as well.

Funding. National Key Research and Development Program of China (2018YFB2201802); National Natural Science Foundation of China (61771285).

Disclosures. The authors declare no conflicts of interest.

REFERENCES

1. M. Seimetz, "Laser linewidth limitations for optical systems with high-order modulation employing feed forward digital carrier phase estimation," in *Optical Fiber Communication Conference/National Fiber Optic Engineers Conference* (Optical Society of America, 2008), paper OTuM2.
2. J. Labaziewicz, P. Richerme, K. R. Brown, I. L. Chuang, and K. Hayasaka, "Compact, filtered diode laser system for precision spectroscopy," Opt. Lett. **32**, 572–574 (2007).
3. Y.-H. Lai, M.-G. Suh, Y.-K. Lu, B. Shen, Q. Yang, H. Wang, J. Li, S. H. Lee, K. Y. Yang, and K. Vahala, "Earth rotation measured by a chip-scale ring laser gyroscope," Nat. Photonics **14**, 345–349 (2020).
4. Z. L. Newman, V. Maurice, T. Drake, J. R. Stone, T. C. Briles, D. T. Spencer, C. Fredrick, Q. Li, D. Westly, B. R. Ilic, B. Shen, M.-G. Suh, K. Y. Yang, C. Johnson, D. M. S. Johnson, L. Hollberg, K. J. Vahala, K. Srinivasan, S. A. Diddams, J. Kitching, S. B. Papp, and M. T.

Hummon, "Architecture for the photonic integration of an optical atomic clock," Optica **6**, 680–685 (2019).
5. J. Li, H. Lee, and K. J. Vahala, "Microwave synthesizer using an on-chip Brillouin oscillator," Nat. Commun. **4**, 2097 (2013).
6. "Continuous wave single frequency IR laser NPRO 125/126 series," https://www.lumentum.com/en/products/laser-solid-state-cw-1064-1319-npro.
7. "Koheras adjustik e15," https://www.nktphotonics.com/wp-content/uploads/sites/3/2015/04/koheras-adjustik-e15.pdf?1550069496.
8. M. Tran Anh, D. Huang, and J. Bowers, "Tutorial on narrow linewidth tunable semiconductor lasers using Si/III-V heterogeneous integration," APL Photon. **4**, 111101 (2019).
9. K.-J. Boller, A. Rees, Y. Fan, J. Mak, R. Lammerink, C. Franken, P. van der Slot, D. Marpaung, C. Fallnich, J. Epping, R. Oldenbeuving, D. Geskus, R. Dekker, I. Visscher, R. Grootjans, C. Roeloffzen, M. Hoekman, E. Klein, A. Leinse, and R. Heideman, "Hybrid integrated semiconductor lasers with silicon nitride feedback circuits," Photonics **7**, 4 (2019).
10. D. Huang, M. Tran Anh, J. Guo, J. Peters, T. Komljenovic, P. Morton, and J. Bowers, "High-power sub-kHz linewidth lasers fully integrated on silicon," Optica **6**, 745–752 (2019).
11. M. L. Davenport, S. Liu, and J. E. Bowers, "Integrated heterogeneous silicon/III-V mode-locked lasers," Photon. Res. **6**, 468–478 (2018).
12. A. Verdier, G. de Valicourt, R. Brenot, H. Debregeas, P. Dong, M. Earnshaw, H. Carrère, and Y. Chen, "Ultrawideband wavelength-tunable hybrid external-cavity lasers," J. Lightwave Technol. **36**, 37–43 (2018).
13. N. Kobayashi, K. Sato, M. Namiwaka, K. Yamamoto, S. Watanabe, T. Kita, H. Yamada, and H. Yamazaki, "Silicon photonic hybrid ring-filter external cavity wavelength tunable lasers," J. Lightwave Technol. **33**, 1241–1246 (2015).
14. Y. Fan, A. van Rees, P. J. M. van der Slot, J. Mak, R. M. Oldenbeuving, M. Hoekman, D. Geskus, C. G. H. Roeloffzen, and K.-J. Boller, "Hybrid integrated InP-Si_3N_4 diode laser with a 40-Hz intrinsic linewidth," Opt. Express **28**, 21713–21728 (2020).
15. Y. Zhu, S. Zeng, and L. Zhu, "Optical beam steering by using tunable, narrow-linewidth butt-coupled hybrid lasers in a silicon nitride photonics platform," Photon. Res. **8**, 375–380 (2020).
16. Y. Fan, R. M. Oldenbeuving, C. G. Roeloffzen, M. Hoekman, D. Geskus, R. G. Heideman, and K.-J. Boller, "290 Hz intrinsic linewidth from an integrated optical chip-based widely tunable InP-Si_3N_4 hybrid laser," in *Conference on Lasers and Electro-Optics* (Optical Society of America, 2017), paper JTh5C.9.
17. A. Gil-Molina, O. Westreich, Y. Antman, X. Ji, A. L. Gaeta, and M. Lipson, "Robust hybrid III-V/Si_3N_4 laser with kHz-linewidth and GHz-pulling range," in *Conference on Lasers and Electro-Optics* (Optical Society of America, 2020), paper STu3M.4.
18. B. Stern, X. Ji, A. Dutt, and M. Lipson, "Compact narrow-linewidth integrated laser based on a low-loss silicon nitride ring resonator," Opt. Lett. **42**, 4541–4544 (2017).
19. Y. Li, Y. Zhang, H. Chen, S. Yang, and M. Chen, "Tunable self-injected Fabry–Perot laser diode coupled to an external high-*Q* Si_3N_4/SiO_2 microring resonator," J. Lightwave Technol. **36**, 3269–3274 (2018).
20. M. J. R. Heck, J. F. Bauters, M. L. Davenport, D. T. Spencer, and J. E. Bowers, "Ultra-low loss waveguide platform and its integration with silicon photonics," Laser Photon. Rev. **8**, 667–686 (2014).
21. C. Xiang, W. Jin, J. Guo, C. Williams, A. M. Netherton, L. Chang, P. A. Morton, and J. E. Bowers, "Effects of nonlinear loss in high-*Q* Si ring resonators for narrow-linewidth III-V/Si heterogeneously integrated tunable lasers," Opt. Express **28**, 19926–19936 (2020).
22. A. Leinse, R. G. Heideman, E. J. Klein, R. Dekker, C. G. H. Roeloffzen, and D. A. I. Marpaung, "Triplex™ platform technology for photonic integration: applications from UV through NIR to IR," in *ICO International Conference on Information Photonics* (IEEE, 2011), pp. 1–2.
23. N. M. Kondratiev, V. E. Lobanov, A. V. Cherenkov, A. S. Voloshin, N. G. Pavlov, S. Koptyaev, and M. L. Gorodetsky, "Self-injection locking of a laser diode to a high-*Q* WGM microresonator," Opt. Express **25**, 28167–28178 (2017).
24. W. Liang, V. Ilchenko, D. Eliyahu, A. Savchenkov, A. Matsko, D. Seidel, and L. Maleki, "Ultralow noise miniature external cavity semiconductor laser," Nat. Commun. **6**, 7371 (2015).
25. W. Liang, V. S. Ilchenko, A. A. Savchenkov, A. B. Matsko, D. Seidel, and L. Maleki, "Whispering-gallery-mode-resonator-based ultranarrow linewidth external-cavity semiconductor laser," Opt. Lett. **35**, 2822–2824 (2010).
26. A. Li, T. Van Vaerenbergh, P. De Heyn, P. Bienstman, and W. Bogaerts, "Backscattering in silicon microring resonators: a quantitative analysis," Laser Photon. Rev. **10**, 420–431 (2016).
27. S. Darmawan, Y. M. Landobasa, and M. Chin, "Pole–zero dynamics of high-order ring resonator filters," J. Lightwave Technol. **25**, 1568–1575 (2007).
28. M. Huang, S. Li, M. Xue, L. Zhao, and S. Pan, "Flat-top optical resonance in a single-ring resonator based on manipulation of fast- and slow-light effects," Opt. Express **26**, 23215–23220 (2018).
29. G. T. Paloczi, J. Scheuer, and A. Yariv, "Compact microring-based wavelength-selective inline optical reflector," IEEE Photon. Technol. Lett. **17**, 390–392 (2005).
30. J. Zhu, K. S. Ozdemir, Y.-F. Xiao, L. Li, L. He, D.-R. Chen, and L. Yang, "On-chip single nanoparticle detection and sizing by mode splitting in an ultrahigh-*Q* microresonator," Nat. Photonics **4**, 46–49 (2010).
31. R. R. Galiev, N. M. Kondratiev, V. E. Lobanov, A. B. Matsko, and I. A. Bilenko, "Optimization of laser stabilization via self-injection locking to a whispering-gallery-mode microresonator," Phys. Rev. Appl. **14**, 014036 (2020).
32. J. F. Bauters, M. J. R. Heck, D. John, D. Dai, M.-C. Tien, J. S. Barton, A. Leinse, R. G. Heideman, D. J. Blumenthal, and J. E. Bowers, "Ultra-low-loss high-aspect-ratio Si_3N_4 waveguides," Opt. Express **19**, 3163–3174 (2011).
33. W. Jin, Q.-F. Yang, L. Chang, B. Shen, H. Wang, M. A. Leal, L. Wu, A. Feshali, M. Paniccia, K. J. Vahala, and J. E. Bowers, "Hertz-linewidth semiconductor lasers using CMOS-ready ultra-high-*Q* microresonators," arXiv:2009.07390 (2020).
34. M. W. Puckett, K. Liu, N. Chauhan, Q. Zhao, N. Jin, H. Cheng, J. Wu, R. O. Behunin, P. T. Rakich, K. D. Nelson, and D. J. Blumenthal, "422 million *Q* planar integrated all-waveguide resonator with a 3.4 billion absorption limited *Q* and sub-MHz linewidth," arXiv:2009.07428 (2020).
35. J. Li, Z. Liu, Q. Geng, S. Yang, H. Chen, and M. Chen, "Method for suppressing the frequency drift of integrated microwave photonic filters," Opt. Express **27**, 33575–33585 (2019).
36. T. Zhu, Y. Hu, P. Gatkine, S. Veilleux, J. Bland-Hawthorn, and M. Dagenais, "Ultrabroadband high coupling efficiency fiber-to-waveguide coupler using Si_3N_4/SiO_2 waveguides on silicon," IEEE Photon. J. **8**, 7102112 (2016).
37. R. Marchetti, C. Lacava, L. Carroll, K. Gradkowski, and P. Minzioni, "Coupling strategies for silicon photonics integrated chips," Photon. Res. **7**, 201–239 (2019).
38. S. Camatel and V. Ferrero, "Narrow linewidth CW laser phase noise characterization methods for coherent transmission system applications," J. Lightwave Technol. **26**, 3048–3055 (2008).
39. L. B. Mercer, "1/f frequency noise effects on self-heterodyne linewidth measurements," J. Lightwave Technol. **9**, 485–493 (1991).
40. P. Laurent, A. Clairon, and C. Breant, "Frequency noise analysis of optically self-locked diode lasers," IEEE J. Quantum Electron. **25**, 1131–1142 (1989).
41. H. Li and N. B. Abraham, "Power spectrum of frequency noise of semiconductor lasers with optical feedback from a high-finesse resonator," Appl. Phys. Lett. **53**, 2257–2259 (1988).
42. N. Schunk and K. Petermann, "Numerical analysis of the feedback regimes for a single-mode semiconductor laser with external feedback," IEEE J. Quantum Electron. **24**, 1242–1247 (1988).
43. C. Henry, "Theory of the linewidth of semiconductor lasers," IEEE J. Quantum Electron. **18**, 259–264 (1982).
44. E. Dale, W. Liang, D. Eliyahu, A. A. Savchenkov, V. S. Ilchenko, A. B. Matsko, D. Seidel, and L. Maleki, "Ultra-narrow line tunable semiconductor lasers for coherent lidar applications," in *Imaging and Applied Optics* (Optical Society of America, 2014), paper JTu2C.3.
45. L. Stern, W. Zhang, L. Chang, J. Guo, C. Xiang, M. A. Tran, D. Huang, J. D. Peters, D. Kinghorn, J. E. Bowers, and S. B. Papp, "Ultra-precise optical-frequency stabilization with heterogeneous III–V/Si lasers," Opt. Lett. **45**, 5275–5278 (2020).

46. B. Shen, L. Chang, J. Liu, H. Wang, Q.-F. Yang, C. Xiang, R. Wang, J. He, T. Liu, W. Xie, J. Guo, D. Kinghorn, L. Wu, Q.-X. Ji, T. Kippenberg, K. Vahala, and J. Bowers, "Integrated turnkey soliton microcombs," Nature **582**, 365–369 (2020).
47. A. Li and W. Bogaerts, "Using backscattering and backcoupling in silicon ring resonators as a new degree of design freedom," Laser Photon. Rev. **13**, 1800244 (2019).
48. A. Li and W. Bogaerts, "Reconfigurable nonlinear nonreciprocal transmission in a silicon photonic integrated circuit," Optica **7**, 7–14 (2020).
49. K. Y. Yang, J. Skarda, M. Cotrufo, A. Dutt, G. Ahn, M. Sawaby, D. Vercruysse, A. Arbabian, S. Fan, A. Alù, and J. Vuckovic, "Inverse-designed non-reciprocal pulse router for chip-based lidar," Nat. Photonics **14**, 369–374 (2020).